Using LES in a Discontinuous Galerkin method with constant and dynamic SGS models

Matthew J. Brazell * Michael Brazell † Michael Stoellinger ‡ Dimitri J. Mavriplis § Andrew Kirby ¶
Department of Mechanical Engineering, University of Wyoming, Laramie WY 82071, USA

The Discontinuous Galerkin (DG) method provides numerical solutions of the Navier-Stokes equations with high order of accuracy in complex geometries and allows for highly efficient parallelization algorithms. These attributes make the DG method highly attractive for large eddy simulation (LES). The main goal of this work is to investigate the feasibility of adopting an explicit filter to the numerical solution of the Navier-Stokes equations to increase the numerical stability of underresolved simulations such as LES and to use the explicit filter in dynamic subgrid scale (SGS) models for LES. The explicit filter takes advantage of DG's framework where the solution is approximated using a polynomial basis. The higher modes of the solution correspond to a higher order polynomial basis, therefore by removing high order modes the filtered solution contains only lower frequency content. The explicit filter is successfully used here to remove the effects of aliasing in underresolved simulations of the Taylor-Green vortex case at a Reynolds number $Re = 1600$. The de-aliasing is achieved by evaluating a solution at a higher order polynomial (effectively increasing the number of quadrature points used for integration) and then projecting the solution down to a lower order polynomial. The SGS models investigated include the constant coefficient Smagorinsky Model (CCSM), Dynamic Smagorinsky Model (DSM), and Dynamic Heinz Model (DHM). The Taylor-Green Vortex case exhibits a laminar-turbulent transition and it is shown that the dynamic SGS models capture this transition more accurately than the CCSM when a sufficiently high polynomial order is used. The explicit test-filter operation for the dynamic models introduces a commutation error. A brief comparison of the effects of the commutative error that exists with this filter implementation is shown although further investigation is needed to determine the more appropriate order of operations.

I. Introduction

Direct Numerical Simulations (DNS) resolves all velocity, length, and time scales in a turbulent flow and are thus computationally too expensive for all but simple problems at low Reynolds numbers. In Large Eddy Simulation (LES), only the large scales of turbulence are resolved and the small scales are modeled. Both DNS and LES require many degrees of freedom and high order methods provide accurate solutions with relatively fewer degrees of freedom compared to low order methods. Spectral methods are commonly used in DNS simulations but they are limited to periodic Cartesian grid problems. Therefore, they are too

*Graduate Student, AIAA Member
†Post Doctoral Research Associate, AIAA Member
‡Assistant Professor, AIAA Member
§Professor, AIAA Fellow
¶Graduate Student, AIAA Member

restricting since most problems of technical interest require an unstructured mesh (e.g. flow over airfoils). The Finite element method is a high order method that can handle unstructured meshes, this allows for high order accuracy within complex geometries. The particular Finite Element method used in this work is a Discontinuous Galerkin (DG) method. DG is used to discretize the compressible LES Navier-Stokes equations. The LES equations are obtained by applying a spatial filter (or a spectral low-pass filter) to the Navier-Stokes equations such that the small scales of turbulent motion are filtered out and the effect of these so called subgrid scales (SGS) are modeled by an additional subgrid scale viscosity. This means that by definition LES is an under-resolved simulation. For spectral methods it is well known that the effect of aliasing[1] in the non-linear convective term can cause numerical instabilities through an accumulation of energy at the high modes. The effect of aliasing can be reduced and the simulation stabilized by adopting an explicit filter operation on the solution.[2,3] In this work we will first investigate the feasibility of polynomial-dealiasing using a sharp cut-off filter in modal space for so called implicit LES (ILES) where no SGS model is used. Then we will investigate the performance of three SGS models: the Smagorinsky model[4] (constant coefficient and dynamic) and a dynamic model developed by Heinz.[5] The constant coefficient Smagorinsky model (CCSM) requires the specification of the model coefficient C_s and the scalar filter scale Δ of the low-pass filter operation that is used to derive the LES equations. With most lower order LES investigations using finite volume or finite difference methods, the low-pass filter operation is not explicitly performed. Instead, it is assumed that the numerical discretization of the derivatives acts as a filter similar to a top-hat filter in space with a filter scale Δ that is equal to the grid spacing δ_x. For the finite volume method the definition is usually given by[4] $\Delta = V_c^{1/3}$ where V_c is the cell volume. In high order DG methods, using the cubic root definition is not appropriate since each DG element approximates the solution to a high order and hence it is not clear what expression should be used to obtain Δ from the element size and polynomial order. A second problem with the CCSM model is that the model coefficient C_s is flow dependent and hence different values are required for different flows. More over, the CCSM model does not perform well in flows that transition from the laminar to the turbulent state. For such flows, the CCSM model predicts a SGS viscosity in all flows with velocity gradients and this added SGS viscosity usually delays the laminar - turbulent transition significantly. The dynamic Smagorinsky model (DSM) was developed to remedy the weaknesses of the CCSM model. In the DSM the model coefficient is calculated based on the flow state and is no longer a model input. The DSM requires the explicit application of a so called test filter operation that is used to determine the model coefficient locally based on turbulence scaling laws. The dynamic model developed by Heinz[5] (DHM) is also based on a test filter operation and is derived from an underlying stochastic turbulence model leading to improved predictions compared to the DSM for certain flows.[5] In theory, the dynamic models should be able to predict laminar - turbulent transition if the dynamic procedure in a laminar flow results in $C_s = 0$ and hence a negligible SGS viscosity. We will investigate the suitability of using the sharp cut-off filter in modal space as a test filter for the dynamic models and evaluate their model performance compared to the CCSM. The flow under consideration is the Taylor Green Vortex test case[6] at a Reynolds number of $Re = 1600$. At this Reynolds number, the flow transitions from an initially laminar vortical flow (prescribed by an analytical velocity field) to a turbulent flow not dissimilar to freely decaying grid generated turbulence. The flow is thus very challenging for any SGS model.

II. Numerical Formulation

A. Discontinuous Galerkin Solver

The governing equations are the compressible Navier- Stokes equations representing the conservation of mass, momentum, and energy and are given by:

$$\frac{\partial}{\partial t}\begin{bmatrix}\rho\\ \rho u\\ \rho v\\ \rho w\\ \rho E\end{bmatrix}+\frac{\partial}{\partial x}\begin{bmatrix}\rho u\\ \rho u^2+p-\tau_{11}\\ \rho uv-\tau_{21}\\ \rho uw-\tau_{31}\\ \rho uH-\tau_{1i}u_i+q_1\end{bmatrix}+\frac{\partial}{\partial y}\begin{bmatrix}\rho v\\ \rho uv-\tau_{12}\\ \rho v^2+p-\tau_{22}\\ \rho vw-\tau_{32}\\ \rho vH-\tau_{2i}u_i+q_2\end{bmatrix}+\frac{\partial}{\partial z}\begin{bmatrix}\rho w\\ \rho uw-\tau_{13}\\ \rho vw-\tau_{23}\\ \rho w^2+p-\tau_{33}\\ \rho wH-\tau_{3i}u_i+q_3\end{bmatrix}=0,$$

where ρ is the density, u, v, w are the velocity components in each spatial coordinate direction, p is the pressure, E is total internal energy, $H = E + p/\rho$ is the total enthalpy, τ is the viscous stress tensor, and q is the heat flux. The viscosity is a function of the temperature given by Sutherland's formula. These equations are closed using the ideal gas equation of state:

$$\rho E = \frac{p}{\gamma - 1} + \frac{1}{2}\rho(u^2 + v^2 + w^2)$$

where $\gamma = 1.4$ is the ratio of specific heats. In all of the following, Einstein notation is used where the subscript i represent spatial dimensions and has a range of 1 to 3. The solution vector is comprised of the conservative variables and is shown under the time derivative.[7]

Discontinuous Galerkin (DG) methods combine ideas of finite element and finite volume methods allowing for high-order approximations and geometric flexibility. This solver utilizes Lax-Friedrichs[8] method for the inviscid flux routine and a symmetric interior penalty (SIP)[9,10] viscous flux routine. The governing equations are marched in time using an explicit 4-stage (fourth order) Runge Kutta method.[11] If used as an LES solver with an SGS model the SGS viscosity is simply added to the molecular viscosity and the viscous flux contains both molecular and turbulence contributions. The intent of this code is to be used as a far body solver with over-set capabilities and it is designed for high speed performance and robustness capable of only structured Hexahedron meshes. DG is a subset of the Finite-Element Method where each element is projected from physical space to a reference space. A polynomial basis is used to approximate the solution in the projected reference space. All basis are equivalent however it is often advantageous to pick a basis for certain characteristics. The basis used for this solver is the Lagrange Nodal basis evaluated at Gauss Lobatto Quadrature points[12] and the number of Gauss quadrature points ngp is related to the polynomial degree of approximation by $ngp = P + 1$. The basis and test function are created using a tensor product of Lagrange Interpolating polynomials which is a non-hierarchical nodal basis. Polynomial orders of $P = 1$ up to $P = 15$ are considered in this work. A great advantage of the DG method over continuous Spectral Elements is the high parallel efficiency capability, allowing for greatly reduced simulation run times.

B. Filter Implementation in DG

Within the framework of a DG solver, high frequency content of the solution is stored in the higher order modes of the polynomial basis. The Nodal basis used in this solver is not hierarchical, i.e. each mode of the basis contains high order content[13] as can be seen in Figure 1A which shows the basis functions of the nodal basis for $ngp = 4$ (highest polynomial degree $P = 3$). In a hierarchical basis such as the Legendre Modal basis, only the higher order modes contain higher order polynomial degrees as can be seen from Figure 1 B. Filtering in a hierarchical basis is straight forward since specific higher order modes can be damped by multiplying the corresponding solution coefficient with value between 0 and 1. If certain higher order modes

are completely removed and the lower order modes are not affected then one speaks of a sharp modal cut-off filter. Such filters have the nice property that a repeated application of the filter has the same outcome as a single application of the filter. Higher order modes can not directly be removed from a "nodal" basis. By transforming the solution given in a "nodal" basis to a solution given in a "modal" basis the coefficients of the higher order modes can be modified and then the modified coefficients in the "modal" basis are transformed back into the "nodal" basis.[2,3,13]

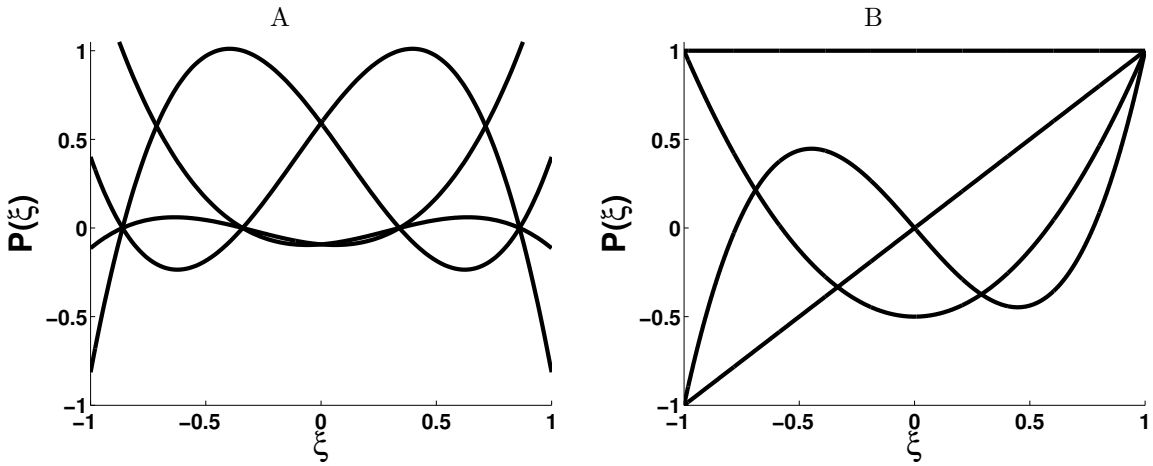

Figure 1. Basis functions up to polynomial degree $P = 3$ for A: the Nodal basis (Gauss-Lobatto Lagrange polynomials) with $ngp = 4$ and B: the Legendre Modal Basis

Here we follow the procedure outlined by Gassner et al.[2] The "nodal" mass matrix $\mathbf{M}$ and solution coefficients b and mixed "modal" mass matrix $\mathbf{C}$ and solution coefficients a are related by

$$U = \mathbf{M}b = \mathbf{C}a,$$

where U denotes the approximation of the solution. We denote the Nodal Basis by $\psi(\xi_i)$, the Modal Basis by $\phi(\xi_i)$, ξ are the Gauss-Lobatto Quadrature Points, and w_k are the Gauss-Lobatto weights associated with each quadrature point. The mass matrices are defined by

$$M_{ij} = \int_{-1}^{1} \psi\psi^T d\Omega = \sum_{k=1}^{ngp} \psi_i(\xi_k)\psi_j(\xi_k)w_k, \tag{1}$$

$$C_{ij} = \int_{-1}^{1} \psi\phi^T d\Omega = \sum_{k=1}^{ngp} \psi_i(\xi_k)\phi_j(\xi_k)w_k. \tag{2}$$

The solution coefficients in the modal basis b are obtained by

$$b = \mathbf{M}^{-1}\mathbf{C}a. \tag{3}$$

Once the coefficients in the Modal Basis b are obtained, the filter operation is simply a matrix vector multiplication

$$\widehat{b} = \mathbf{F}b, \tag{4}$$

where $\mathbf{F}$ is the sparse filter matrix (for the modal basis) and the hat symbol indicates that the coefficients have been filtered. For the sharp modal cut-off filter, the value of $F_{i,i}$ where i is the particular mode to be modified is set to one for all $i \leq P_c$ and is set to zero for all $i > P_c$ where P_c is the desired cut-off mode. By using

$$a = \mathbf{C}^{-1}\mathbf{M}b, \tag{5}$$

and substituting the modal coefficients b with filtered modal coefficients $\widehat{b}$ gives the filtered solution coefficients $\widehat{a}$ in the nodal basis

$$\widehat{a} = \mathbf{C}^{-1}\mathbf{M}\left(\mathbf{F}b\right). \tag{6}$$

By introducing the matrices

$$\mathbf{B} = \mathbf{C}^{-1}\mathbf{M}, \;\; \mathbf{B}^{-1} = \mathbf{M}^{-1}\mathbf{C}, \tag{7}$$

and

$$\widehat{F} = \mathbf{B}^{-1}\mathbf{F}\mathbf{B}, \tag{8}$$

we can finally write the sharp modal cut-off filter operation as

$$\widehat{a} = \widehat{\mathbf{F}}a. \tag{9}$$

It is worth noting that the modified filter matrix $\widehat{\mathbf{F}}$ can be assembled as a pre-processing step and does not have to be recalculated during the simulation. Fig. 2 shows a simple 1-D example of the modal filtering approach. We use a function f that has a low and high frequency content $f(x) = cos(2.*x) + 0.3*sin(8*x)$ (black line) on the interval $[-\pi, \pi]$. The function is well approximated by DG (green line) on $N = 6$ elements with a polynomial degree $P = 4$ (hence using $ngp = 5$ quadrature points shown as green dots). The discontinuous nature of the approximation is also clearly visible by the "jumps" of the approximation at the element boundaries. Applying the sharp modal cut-off filter so that modes with polynomial degree larger than one are removed ($P_c = 1$) leads to the piece-wise linear approximation indicated by the red line in fig. 2. Clearly, the sharp modal cut-off filter is able to remove the high frequency content of the function f.

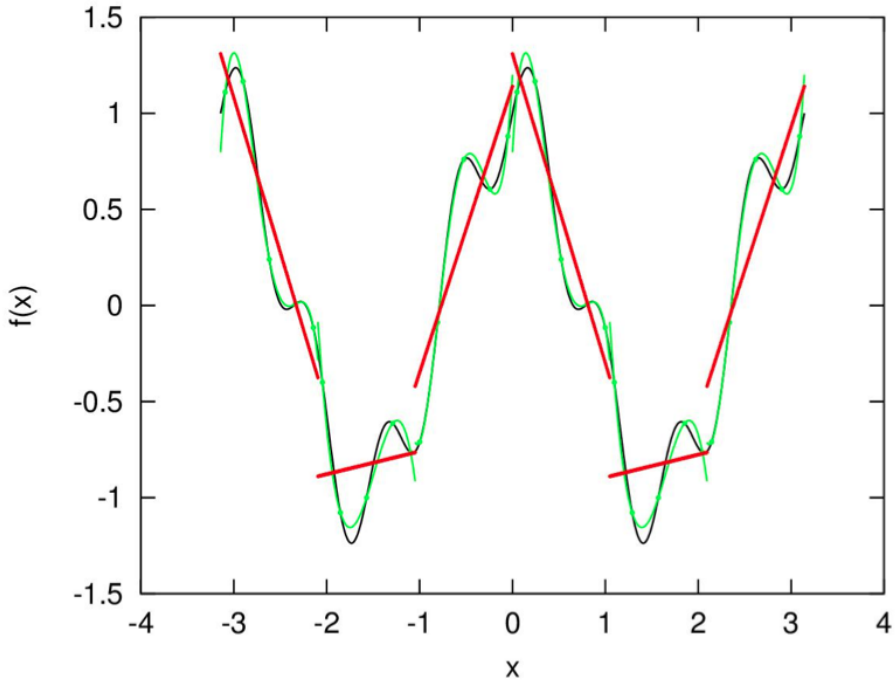

Figure 2. One dimensional example of the sharp spectral cut-off filter. Original function $f(x) = cos(2.*x) + 0.3*sin(8*x)$ (black line), DG approximation on $N = 6$ elements with fourth order polynomials $P = 4$ (green line, dots represent the $ngp = 5$ quadrature points on each element), and filtered solution using the sharp spectral cut-off filter with $P_c = 1$ and $N = 6$ elements (red line).

C. Polynomial dealiasing using a sharp modal cut-off filter

Polynomial aliasing occurs in under resolved simulations due to the quadrature errors that are introduced when calculating inner products of the non-linear convective terms in the Navier-Stokes Equations.[1] The errors can lead to a build up of energy in the higher order modes and hence lead to instabilities of the simulations. For DG simulations with lower polynomial orders there seems to be sufficient numerical dissipation such that the energy in the higher order modes is dissipated sufficiently fast.[2,3] For higher polynomial approximations which are more desirable from a convergence point of view and also for better parallel efficiency the numerical dissipation is greatly reduced and not sufficient to remove the aliasing errors. One method to prevent polynomial aliasing is to use more quadrature points in the evaluation of the inner products of the non-linear terms. However, this would require a significant alteration of the DG code. A second more straight forward method is to increase the number of solution quadrature points for all solution operations by increasing P (P+1 quadrature points) and then projecting the solution back to a lower order P_c by applying the sharp modal cut-off filter. We will apply this method for polynomial dealiasing to test the implementation of the modal cut-off filter (which will later also be used for the dynamic SGS models). This polynomial dealiasing approach has previously been adopted by Laslo et al[3] and Gassner et al.[2] In the context of LES, polynomial dealiasing can be viewed as an explicitly filtered LES. This means that the solution is explicitly filtered at every time step and thereby limiting the spectral content of the solution to a level that is determined by the sharp modal cut-off filter.

III. LES SGS Models considered

A. Smagorinsky Model

The LES equations are obtained by applying a low-pass filter to the Navier-Stokes equations such that the small scales of turbulent motion are filtered out and the effect of these so called subgrid scales on the resolved scales are most commonly modeled by an additional subgrid scale viscosity. The SGS viscosity provides the additional dissipation that occurs in the unresolved small scales. We will denote the low pass-filter operation used to derive the LES equations by an overbar e.g. $\overline{\rho}$ denotes the filtered density. In compressible flows, turbulence modeling is based on density weighted (Favre) filtering[4] for all variables except pressure and density. For example, the Favre filtered velocity is

$$\widetilde{u} = \frac{\overline{\rho u}}{\overline{\rho}}. \tag{10}$$

As mentioned in the introduction, in most LES applications the low-pass filter operation (called the grid filter) is not performed explicitly, but implicitly through the numerical approximation. In this work, we consider cases without using an explicit low-pass filter operation and cases where we us the sharp modal cut-off filter as grid filter. The additional SGS viscosity is defined as

$$\mu_{sgs} = \overline{\rho}(C_s\Delta)^2 \left|\widetilde{S}\right|, \tag{11}$$

where C_s is a model parameter, Δ is the length scale associated with the grid filter and $\widetilde{S}$ is the magnitude of the Favre averaged rate of strain tensor given by

$$\widetilde{S}_{ij} = \frac{1}{2}\left(\frac{\partial \widetilde{u}_i}{\partial x_j} + \frac{\partial \widetilde{u}_j}{\partial x_i}\right), \ \left|\widetilde{S}\right| = \sqrt{2\widetilde{S}_{ij}\widetilde{S}_{ij}}. \tag{12}$$

In the constant coefficient Smagorinsky Model (CCSM) the model parameter is set to $C_s = 0.17$.[14] The commonly used definition of the filter size has to be modified in the high-order DG method considered in this work . Since the DG elements are typically much larger than finite volume cells and resolve much more

detail, the filter width Δ should be defined as a function of the polynomial order of accuracy P. Here we propose the simple approach

$$\Delta = C_p \times (\Delta_x \Delta_y \Delta_z)^{1/3}, \tag{13}$$

where the parameter C_p is estimated to be given by

$$C_p = \frac{1}{2}\frac{1}{P+1}, \tag{14}$$

with P the polynomial order of approximation of the DG elements.

B. Dynamic Smagorinsky Model Definition

In the dynamic Smagorinsky Model[4] (DSM) the Smagorinsky coefficient is calculated based on the local instantaneous flow state and hence $C_s = f(x, y, z, t)$, a function of space and time rather than simply defined as a constant. The dynamic calculation of the coefficient is based on an explicitly performed second level filter operation called the test filter that is applied to the grid filtered variables. We denote the test filter operation by a hat e.g. the test filtered density is denoted by $\widehat{\overline{\rho}}$. Here we always use the sharp modal cut-off filter as the test filter as described in section II.B. The product $(C_s\overline{\Delta})^2$ can be calculated from the ratio

$$(C_s\overline{\Delta})^2 = \frac{1}{2}\frac{L_{ij}^d M_{ij}}{M_{kl}M_{kl}}, \tag{15}$$

where L_{ij}^d is the deviatoric part of the Leonard stress tensor

$$L_{ij} = \widehat{\overline{\rho}\widetilde{u}_i\widetilde{u}_j} - \frac{\widehat{\overline{\rho}\widetilde{u}_i}\,\widehat{\overline{\rho}\widetilde{u}_j}}{\widehat{\overline{\rho}}},\; L_{ij}^d = L_{ij} - \frac{1}{3}L_{kk}\delta_{ij}, \tag{16}$$

and the tensor M_{ij} is given by

$$M_{ij} = \left(\widehat{\overline{\rho}\left|\widetilde{S}\right|\widetilde{S}_{ij}^d}\right) - \alpha\widehat{\overline{\rho}}\left|\widehat{\widetilde{S}}\right|\widehat{\widetilde{S}_{ij}^d}. \tag{17}$$

Since taking the derivative and applying the test filter operation do not commute for the sharp modal cut-off filter one has to agree on the order in which the operations are applied to the second term of M_{ij}. Here we calculate the test filtered velocity first and then calculate the derivatives of the test filtered velocity to form the rate of strain tensor. α denotes the square of the test filter to grid filter width ratio $\alpha = (\frac{\widehat{\overline{\Delta}}}{\overline{\Delta}})^2$. Typically, $\alpha = 4$ since the test filter is often assumed to be twice the width of the grid filter.[14] In the DG method adopted in this work we calculate α using the expression for C_P (14) giving

$$\alpha = \left(\frac{(P_{grid}+1)}{(P_{test}+1)}\right)^2. \tag{18}$$

Here, P_{grid} refers to the polynomial order of the DG method if no explicit grid filter operation is used or to the polynomial order after the explicit grid filter (sharp modal cut-off with $P_{grid} = P_c$ is applied) and P_{test} is the polynomial order after applying the explicit test filter with $P_{test} < P_{grid}$.

By inspecting the expression for $(C_s\overline{\Delta})^2$ one can see that nothing ensures that the numerator will be positive nor that the denominator does not go to zero. The latter issue is simply removed by adding a small number to the denominator. The former issue is more problematic as it would lead to negative SGS viscosity. Physically it has been shown that negative values should occur[5] and they correspond to what is called energy backscatter: energy from the SGS scales is transferred back to the resolved scales. Numerically, negative SGS values destabilize the solution in particular when the sum $\mu + \mu_{sgs}$ becomes negative. To stabilize the DSM, it is customary to either clip the SGS viscosity to positive values or to perform some sort of additional

averaging of the numerator and denominator of equation (15). Here we will consider averaging over the entire DG element (thus providing a single value for $(C_s\overline{\Delta})^2$ per element)

$$(C_s\overline{\Delta})^2 = \frac{1}{2}\frac{\langle L_{ij}^d M_{ij}\rangle}{\langle M_{kl}M_{kl}\rangle}, \tag{19}$$

where the element averaging operator is defined by

$$\langle Q\rangle = \frac{\int_{V_e} Q dV}{V_e}, \tag{20}$$

with V_e the element volume.

C. Dynamic Heinz Model Definition

Similarly to the DSM, the Heinz model[5] (DHM) calculates C_s dynamically as function of space and time. The main difference to the dynamic Smagorinsky model is that now the Leonard stress tensor is modeled. Details of the model derivation can be found in Gopalan and Heinz.[5] The model coefficient in the Heinz model is determined by

$$(C_s\overline{\Delta})^2 = -\frac{L_{ij}\widehat{\overline{S}_{ij}}^d}{\alpha\left|\widehat{\overline{S}}^d\right|^3}$$

The implementation of this model in typical finite difference and finite volume solvers has shown improved results achieved with less stringent clipping or averaging of $(C_s\overline{\Delta})^2$ as compared to the DHM.

IV. Taylor Green (TG) Vortex Flow

The advantage of using the Taylor Green Vortex case is that this flow has the same initialization for every simulation and it is well documented providing a reliable comparison with other codes including DG. The Taylor Green vortex is initially laminar and becomes fully turbulent in later stages making it a challenging test case for dynamic SGS models. A disadvantage is the additional run time to obtain a fully turbulent solution. We will focus on the $Re = 1600$ case for which highly accurate DNS results[6] (obtained with a spectral code using 512 modes) are available for comparison to our DNS (for code validation) and LES model evaluation. Figure 3 shows vorticity contours at the initial condition (left) and towards the end of the run for the spectral DNS.[6]

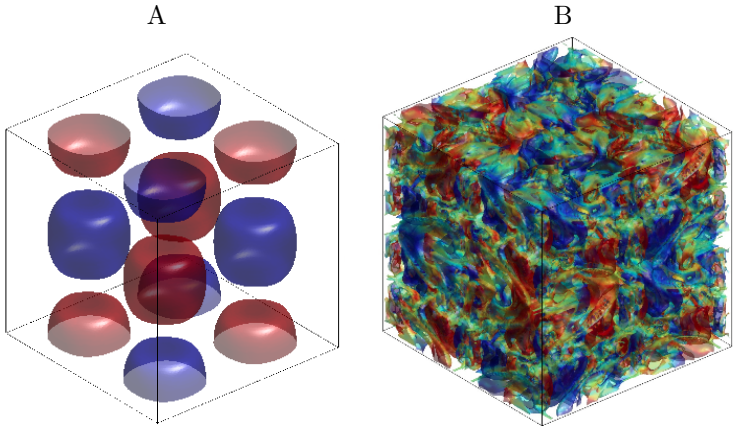

Figure 3. Taylor Green Vortex with Re=1600 showing contours of Z-Vorticity[6] at t=0 (A) and t=20 (B)

The computational domain is given by $\Omega = [-\pi L, \pi L] \times [-\pi L, \pi L] \times [-\pi L, \pi L]$ and periodic boundary conditions are applied in all directions. The Taylor Green Vortex Case was initialized based on the parameters: $L = 1$, $Re = 1600$, $U_0 = 0.1$, $\rho = 1$, $\mu = 6.25 \times 10^{-5}$, $Pr = 0.71$, and $P_0 = 0.714$. These parameters correspond to $Ma = 0.1$ such that the results can be safely compared to the incompressible spectral DNS results.[6] The initial velocity and pressure fields are given by

$$\begin{aligned} u &= U_0 sin(\frac{x}{L}) cos(\frac{y}{L}) cos(\frac{z}{L}), \\ v &= -U_0 cos(\frac{x}{L}) sin(\frac{y}{L}) cos(\frac{z}{L}), \\ w &= 0, \\ p &= p_0 + \frac{\rho_0 V_0^2}{16} \left(cos\left(\frac{2x}{L}\right) + cos\left(\frac{2y}{L}\right) \right) \left(cos\left(\frac{2z}{L}\right) + 2 \right). \end{aligned} \tag{21}$$

Relevant post processing quantities are the kinetic energy

$$E_k(t) = \frac{1}{\rho_0 \Omega} \int_\Omega \rho \frac{u \cdot u}{2} d\Omega, \tag{22}$$

and the kinetic energy dissipation rate

$$\varepsilon(t) = -\frac{dE_k}{dt}. \tag{23}$$

It should be noted here that the dissipation of kinetic energy is calculated from the kinetic energy by using a simple forward difference approximation of the time derivative. Thus, the dissipation rate ε also contains contributions from the numerical dissipation (see Wang et al.[6] for a more detailed discussion about the definition of dissipation rate). Both the dissipation rate and time are normalized for comparison with results from the High Order Workshop.[6] Dissipation is normalized with $\frac{U_0^3}{L}$ and time is normalized with $\frac{L}{U_0}$.

V. Results

A. Code Validation based on the TG vortex flow

The DG solver adopted in this work is validated by performing a DNS of the TG vortex case at $Re = 1600$ through a comparison with results obtained with a fully spectral code using 512^3 modes (= degrees of freedom). For the DG code, degrees of freedom (DOF) can be increased by increasing the polynomial order of accuracy P and/or increasing the number of elements and is defined in 3D as

$$DOF = \left[(P+1)N\right]^3, \tag{24}$$

where P is the polynomial degree and N is number of elements. Figure 4 shows that using 320^3 DOF ($P = 4$, $N = 64$) provides a very close agreement for the dissipation rate compared to the spectral DNS results.[6] Fig. 5 gives an impression of the increase in accuracy for DNS results obtained with varying DOF. It can be seen that reasonable DNS results are obtained for simulations with more than 256^3 degrees of freedom. Figure 6 shows that for the TG vortex when the total number of DOF is fixed, a much greater accuracy of the simulation is obtained by increasing the polynomial order P (called P refinement) instead of increasing the number of elements N (called h refinement).

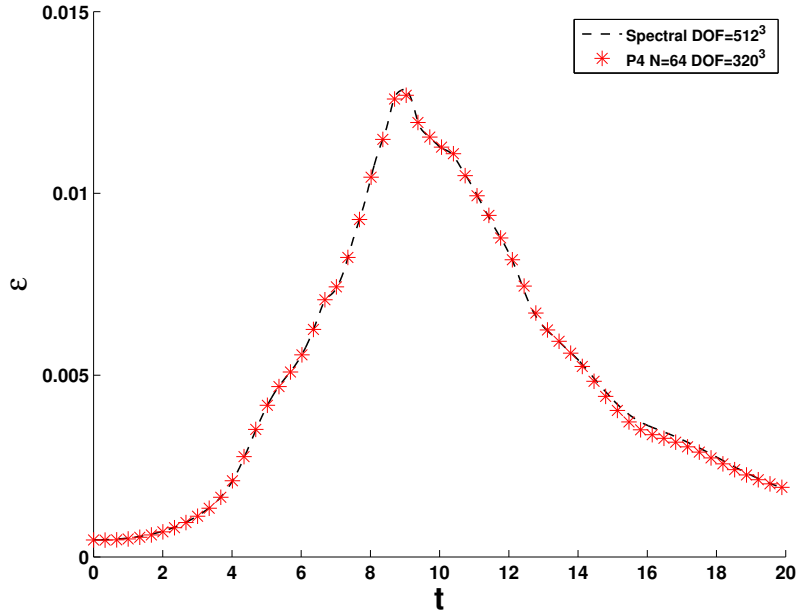

Figure 4. Taylor Green Vortex with Re=1600 Dissipation curve; DG code validation with DNS.

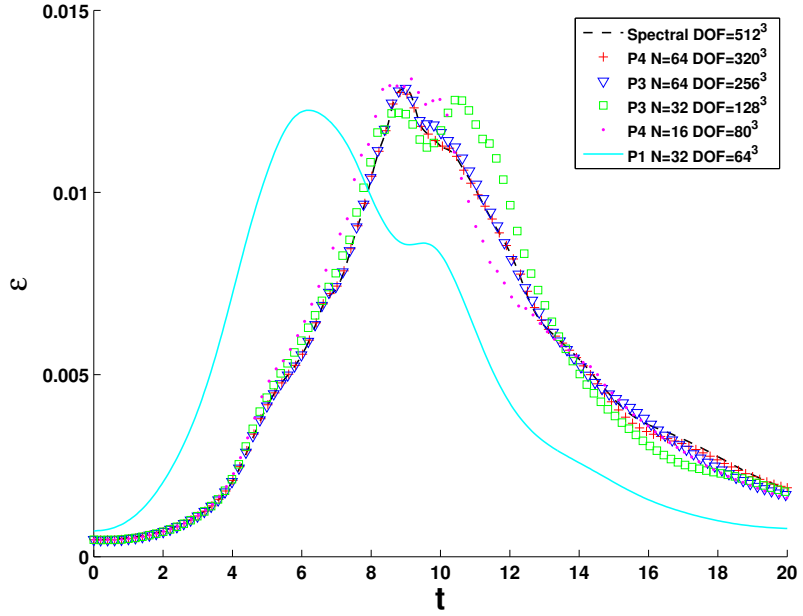

Figure 5. Taylor Green Vortex with Re=1600 Dissipation curve; Comparison of DNS results obtained with increasing degrees of freedom.

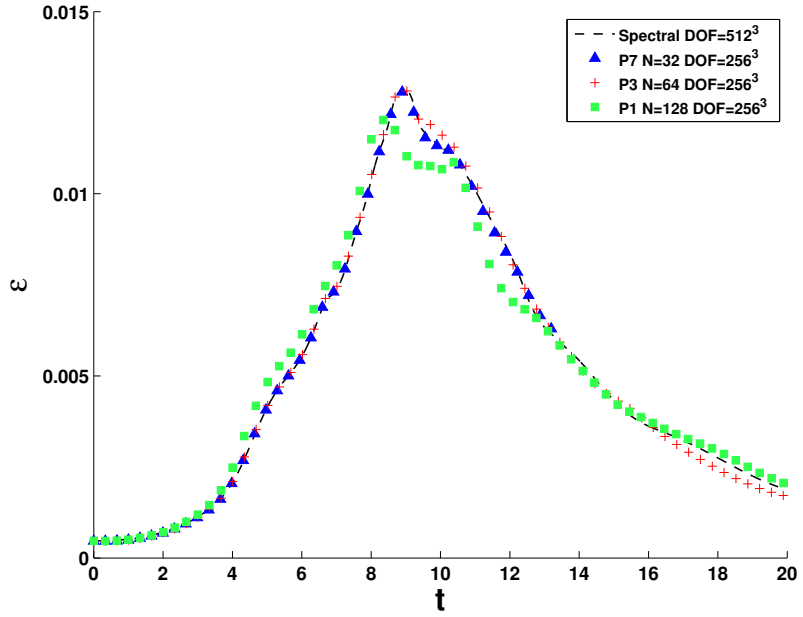

Figure 6. Taylor Green Vortex with Re=1600 Dissipation curve; Comparison of DNS results using P refinement vs. h refinement for a fixed number of 256^3 DOF.

B. Polynomial dealiasing

The work done by Laslo et al.[3] showed that increasing the integration points (Gauss Quadrature Points) can prevent instability from polynomial aliasing errors. The focus of this comparison is to validate the implementation of the sharp modal cut-off filter by demonstrating that the filter can be used as a method of polynomial dealiasing. Fig. 7 A shows simulation results obtained with a fixed number of 64^3 DOF but with different P and N combinations. In the previous section it was shown that it takes more than 256^3 DOF to obtain accurate DNS results. Hence the simulations presented here can be viewed as an under-resolved DNS or as an implicit LES (since no SGS model is adopted). Figure 7A shows that the low order $P = 1$ and $P = 3$ simulations run stable but do not give very accurate results. When the polynomial order is increased further to $P = 7$ the simulation crashes after a third of the runtime. This shows that for under resolved simulations with large P the aliasing error can indeed cause stability problems. Fig. 7B shows results for the corresponding simulations but now with the use of a sharp modal cut-off filter of order P_C chosen such that twice as many quadrature points are used[3] (following the $2N$ rule for dealiasing for compressible flows). The modal cut-off filter operation is applied to the residual at every Runge-Kutta stage. Hardly any difference can be seen for the $P = 1$ and $P = 3$ case due to the dominance of the numerical dissipation. For the $P = 7$ case the effect of the dealiasing is significant since the simulation now runs stable and provides results with a reasonable agreement with the spectral DNS.

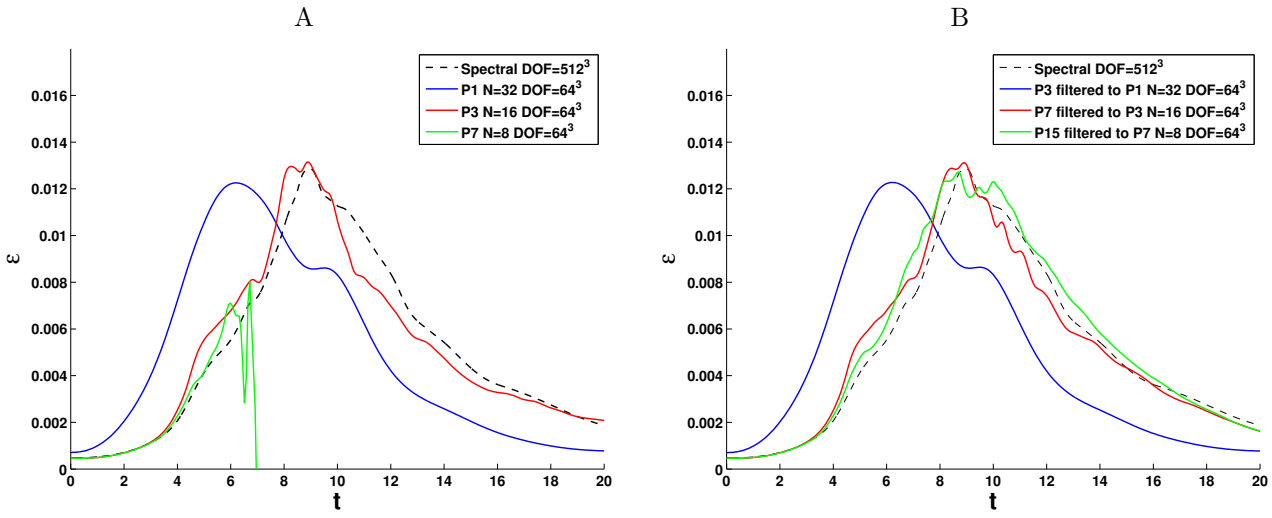

Figure 7. Taylor Green Vortex with Re=1600 Dissipation curve; [A: Effects of Aliasing, B: De-Aliasing by filtering]

Figure 8 shows comparisons of the unfiltered and filtered cases for two different polynomial orders. The figures also show results that have been obtained by adopting the filter only once at the end of the time step (instead of applying the filter at every RK stage). For the two cases it seems to be sufficient to only filter at the end of the time step which leads to a significant reduction of computational cost.

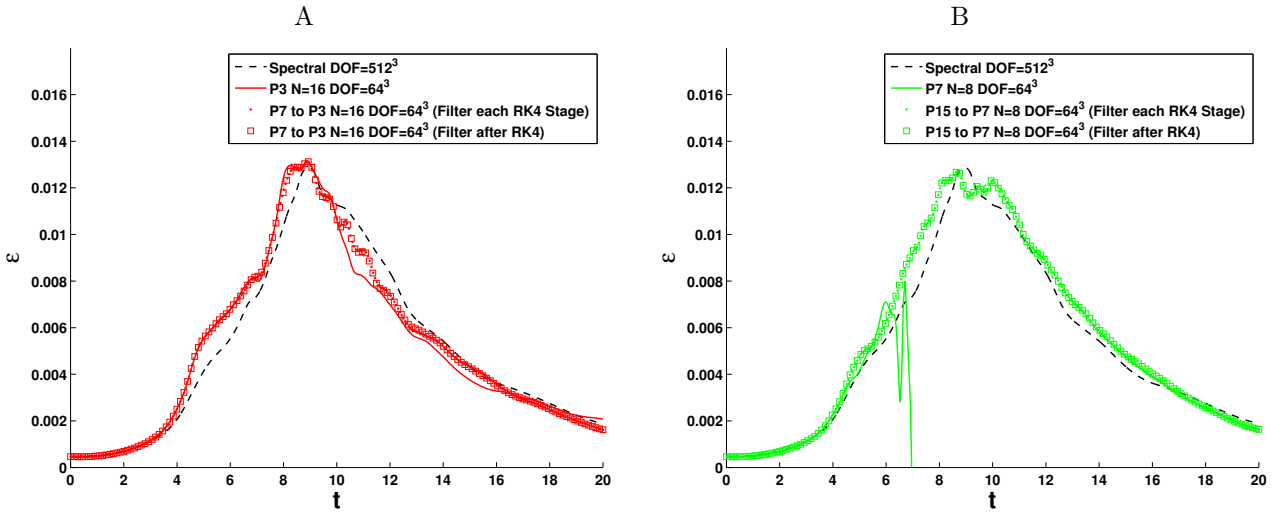

Figure 8. Taylor Green Vortex with Re=1600 Dissipation curve; De-Aliasing Comparison [A: P3 N = 16 64^3 DOF (line: no filter, dot: de-aliasing with P=7 and filtering to P3 at each RK4 Stage, square: de-aliasing with P=7 and filtering to P3 after RK4), B: P7 N = 8 64^3 DOF (line: no filter, dot: de-aliasing with P=15 and filtering to P7 at each RK4 Stage, square: de-aliasing with P=15 and filtering to P7 after RK4)]

C. LES results: SGS model comparison

As described above the dynamic SGS models can produce a negative SGS viscosity and hence cause a numerical instability. Common approaches to ensure stability due to local large negative values from the

SGS models include spatial and temporal averaging of the numerator and denominator making up $(C_S\Delta)^2$ or a clipping of $(C_S\Delta)^2$. In this section, we adopt clipping of large positive and large negative values of the SGS viscosity relative to the laminar viscosity μ_0 such that

$$|\mu_{sgs}| = 3 \cdot \mu_0. \tag{25}$$

Simulations using a mesh with $N = 32$ elements and $P = 3$ (M1) are performed to test several SGS models. The dissipation results are shown in Figure 9. Both DSM and DHM show a slight improvement compared with the no SGS model and CCSM results. Both dynamic models use a test filter with polynomial order $P_c = 1$. The CCSM improves the solution but as expected there is too much dissipation during the first half of the simulation when the flow is laminar. Since the DSM and DHM results are almost identical, the further analysis will be based only on using the DSM. Like many LES model implementations a grid filter was not used explicitly. We expect that explicitly applying a grid filter will lead to improved results and a better connection between the physics and SGS models. For this low order case, clipping μ_{sgs} yields fairly good results. However, the specific clipping values are certainly flow dependent and hence clipping is not a desirable procedure for stabilization and is not considered further.

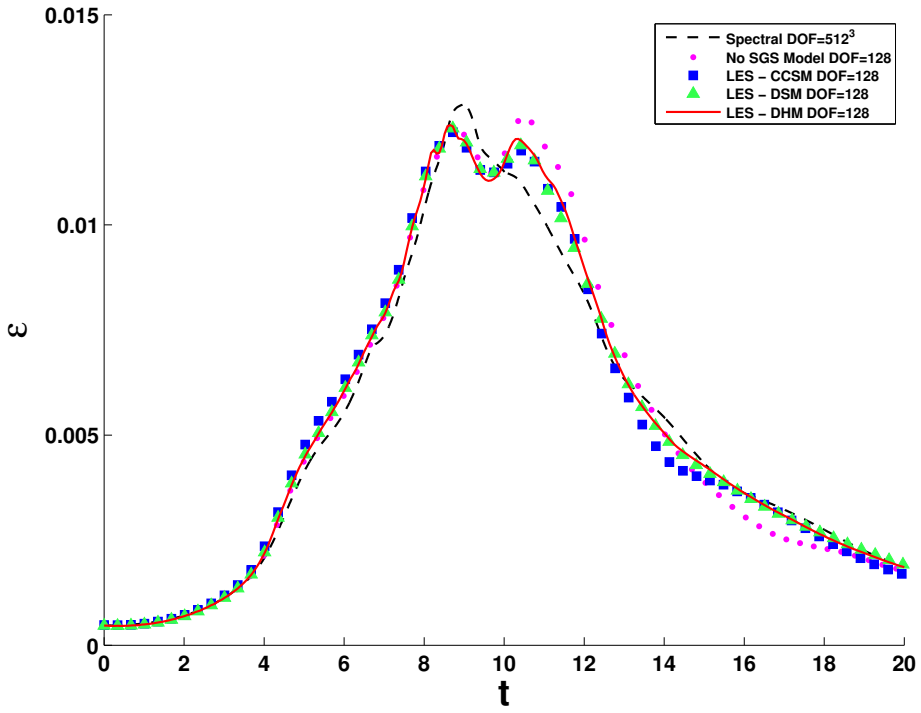

Figure 9. Taylor Green Vortex with Re=1600 Dissipation curve; SGS Model Comparison for mesh M1. The black line represents the spectral method for comparison. Other cases represent 128^2 DOF. No SGS model is shown with magenta dots for comparison as well as the CCSM shown with Blue squares. All dynamic models present clip $\mu_t \pm 3\mu_0$ and test filter P=1. The DSM is shown with Green triangles and the DHM is shown with a red line.

D. LES results: Dynamic procedure based on averages

To avoid the ad-hoc clipping procedure adopted in the preceding section we consider averaging the numerator and denominator of the $(C_s\Delta)^2$ expression locally on each element as described in section B. For the mesh M1 considered in the previous section, the choice for applying a test filter is limited to $P_c \leq 2$. Using $P_c = 1$, the DSM shows only a small improvement compared with the CCSM as shown in Figure 10. This effect is most likely due to the lack of high order content to remove when the test filter is applied. To see if there is

any improvement with a higher order test case a mesh (M2), P=5, 16 elements ($96^3 DOF$) is tested. Mesh M2 has fewer degrees of freedom but is higher order. There is a significant improvement when averaging is used in the DSM in a higher order polynomial case as shown in Figure 11. This finding is more evident when considering the L_2 and L_∞ norm of the difference between dissipation from the spectral method and the DG LES method as shown in Table 1. In particular, the L_2 norm is improved by about 30% with the DSM as compared to the CCSM. Although this is a promising result, the improvement over the no SGS model case is almost negligible. Studying a higher Reynolds number case on the same mesh M2 would result in overall larger contributions from the SGS model and hence we believe that for such a case the dynamic models would provide significantly more accurate results than a simulation with no SGS model.

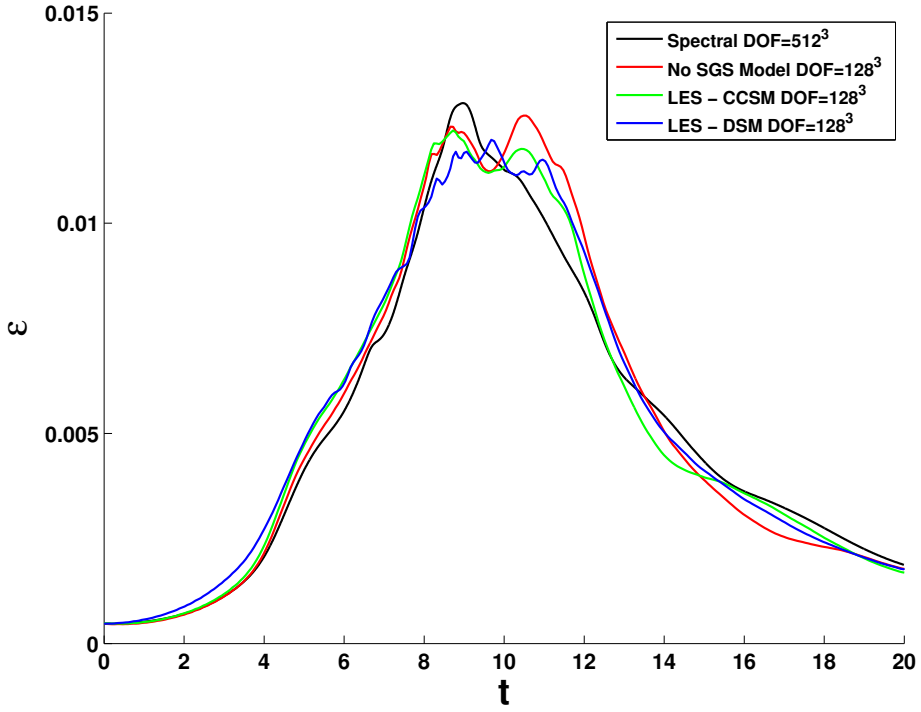

Figure 10. Taylor Green Vortex with Re=1600 Dissipation curve; Comparing Lower Order Case mesh M1 with Spectral method shown by the Black line. All other cases represent $128^3 DOF$. The red line shows no SGS model and the green line shows the CCSM for comparison. The DSM is shown by the Blue line with averaging $(C_s\Delta)^2$ and test filter P=1.

Table 1. Taylor Green Vortex with Re=1600 Dissipation; Comparing L_2 and L_∞ norms for High Order DSM mesh M2

Norm	No SGS Model	Smagorinsky Model	Dyn. Smagorinsky
L_2	0.0174	0.0232	0.0147
L_∞	0.0011	0.0013	0.0011

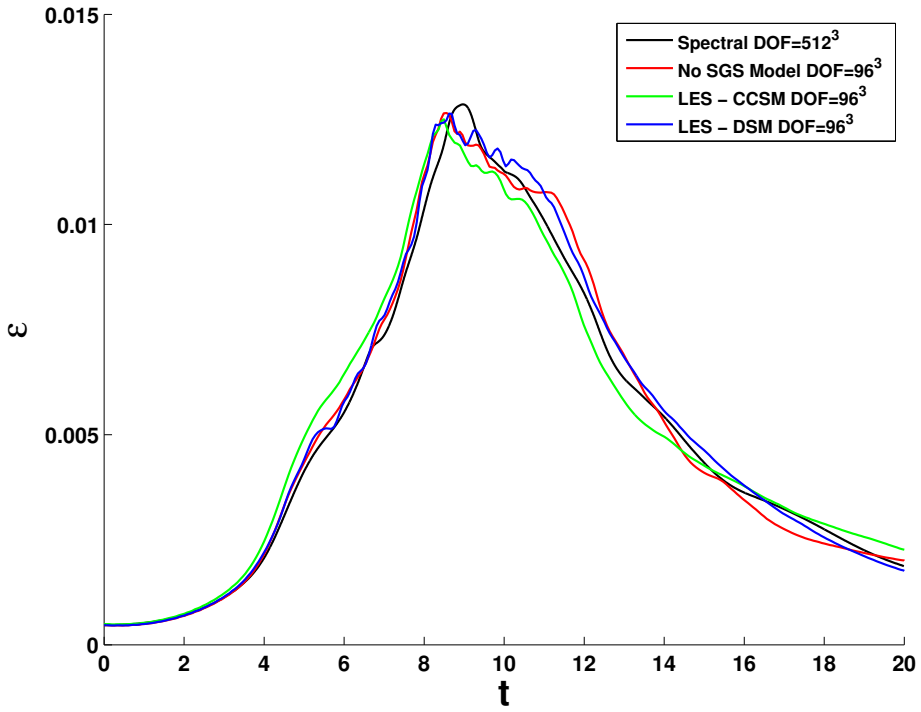

Figure 11. Taylor Green Vortex with Re=1600 Dissipation curve; Comparing Higher Order Case mesh M2 with Spectral method shown by the Black line. All other cases represent $96^3 DOF$. The red line shows no SGS model and the green line shows the CCSM for comparison. The DSM is shown by the Blue line with averaging $(C_s\Delta)^2$ and test filter P=3.

E. LES results: Effect of commutation

The LES method and all the SGS models are derived under the assumption that the filter operation and taking derivatives commute. For the test filter adopted here we know that this commutation is not given. It is thus interesting to investigate if the particular order chosen in section III.B has an influence on the simulation results. Method 1 is associated with filtering the velocity $\widehat{u}$ and then taking the derivative of velocity to form $\frac{\partial \widehat{u_i}}{\partial x_i}$ as explained in section III.B. Method 2 filters the derivative of velocity $\frac{\partial u_i}{\partial x_i}$ to form $\widehat{\frac{\partial u_i}{\partial x_i}}$ as suggested by Blackburn and Schmidt.[13] With the same mesh M2 and using a test filter of P=3, both methods for applying the test filter to $\frac{\partial u_i}{\partial x_i}$ with the DSM show improvement when compared to the CCSM as shown in Figure 12. Method 1 shows somewhat greater improvement based on the L_2 and L_∞ norms given in Table 2. Further analysis is needed to better understand why one method is better than the other.

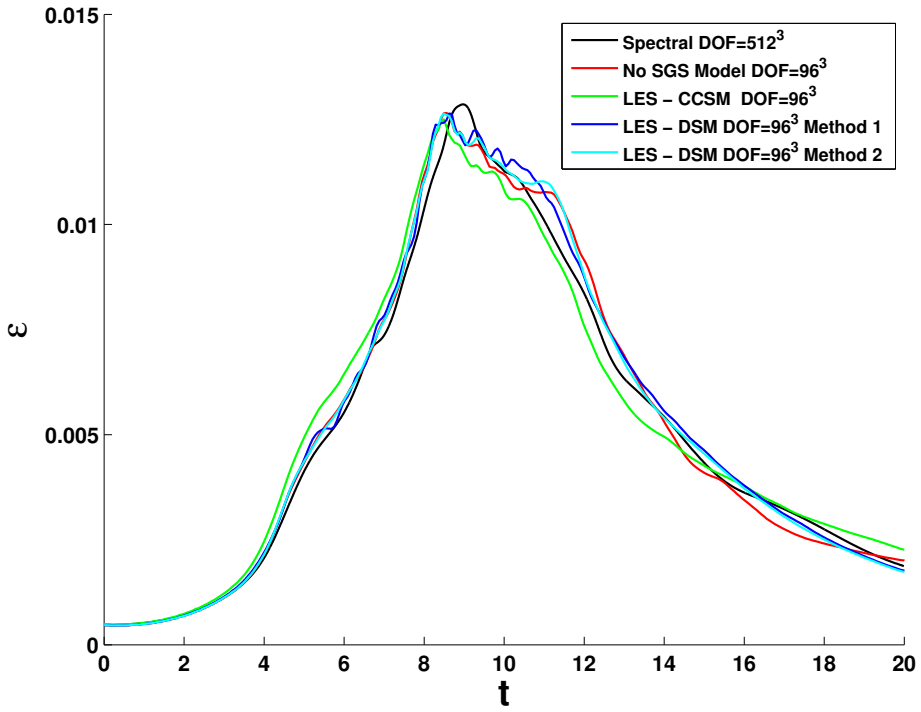

Figure 12. Taylor Green Vortex with Re=1600 Dissipation curve; Comparing the order of filtering and velocity derivative for mesh M2. Spectral method shown for comparison with Black line. All other cases represent $96^3 DOF$. The red line represents no SGS model for comparison and the green line shows CCSM. The other cases show comparison using DSM with two different methods of obtaining a filtered velocity gradient (Blue line: DSM Method 1, Cyan line: DSM Method 2).

Table 2. Taylor Green Vortex with Re=1600 Dissipation; Comparing L_2 and L_∞ norms for two methods of filtering velocity derivatives.

Norm	No SGS Model	CCSM	DSM Method 1	DSM Method 2
L_2	0.0174	0.0232	0.0147	0.0157
L_∞	0.0011	0.0013	0.0011	0.0012

F. LES results: Effect of the test filter order

The effect of choosing the order of the test filter P_c is studied next. This corresponds to choosing the width of the test filter if it where a purely spatial filter procedure. We use the mesh M2 to compare DSM results that have been obtained with different orders of the test filter. It is clear from Figure 13 and Table 3 that using a test filter that is too coarse or not coarse enough is less advantageous than selecting the test filter to retain only half of the modes of the grid filter which in this case corresponds to $P_c = 2$. It is interesting to note that, based on the formula (18), this choice for the test filter leads to a corresponding filter ratio $\frac{\widehat{\overline{\Delta}}}{\overline{\Delta}} = 2$ which is most often adopted in dynamic LES using finite volume or finite difference solvers.

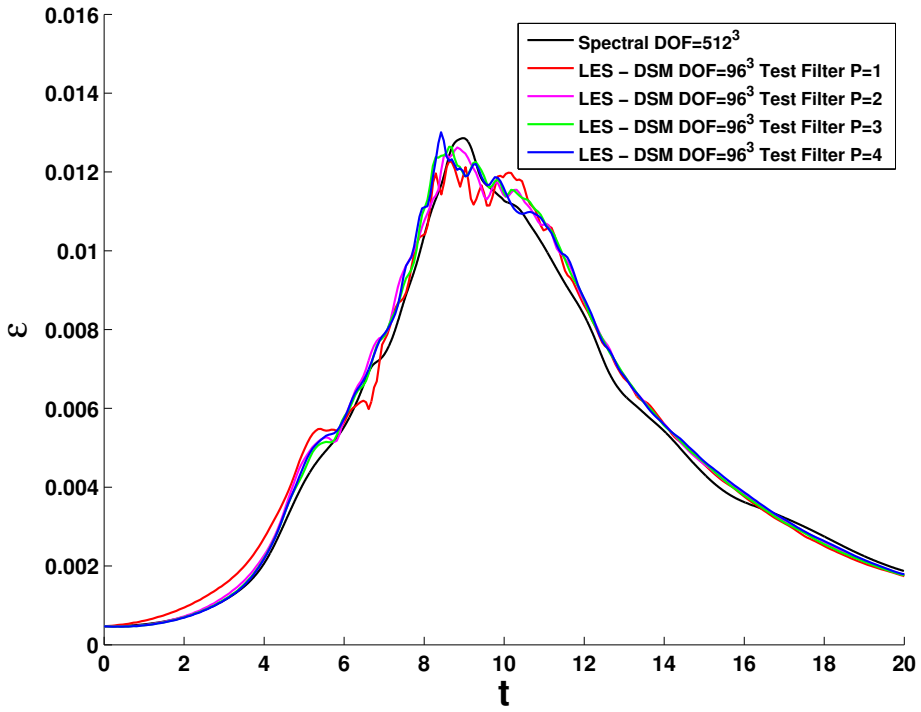

Figure 13. Taylor Green Vortex with Re=1600 Dissipation curve; Compare Test Filter Width for DSM using mesh M2. DSM has a test filter that varies between P=1 to P=4. Spectral method shown for comparison with Black line. Other cases shown represent $96^3 DOF$ with various test filters used (Red: Test Filter P=1, Magenta: Test Filter P=2, Green: Test Filter P=3, Blue: Test Filter P=4)

Table 3. Taylor Green Vortex with Re=1600 Dissipation; Comparing L_2 and L_∞ norms for varying Test Filters for DSM with mesh M2.

Norm	Test Filter P=1	Test Filter P=2	Test Filter P=3	Test Filter P=4
L_2	0.0187	0.0141	0.0147	0.0158
L_∞	0.0013	0.00086	0.0011	0.0013

VI. Conclusion

The main objective of this work is to investigate the feasibility of using dynamic SGS models in a Discontinuous Galerkin method. The DG method allows for high order solutions in complex domains and is thus a very attractive numerical method for LES. The dynamic SGS models all require the use of an explicit filter operation (called the test filter) to determine the model parameters dynamically. It is well known that high order simulations of under-resolved flows (such as LES) can suffer from numerical instability due to aliasing. Modal filters have been used in the past to reduce the aliasing error. Hence, one could use the same filtering approach to reduce aliasing errors and also to perform the explicit test filter operation for the dynamic SGS models. For DG a straight forward method to filter and remove high order content can be achieved by dropping modes of the solution coefficients. The DG solver adopted in this work uses a non-hierarchical Lagrange Nodal basis evaluated at Gauss Lobatto quadrature points, therefore a transformation to another basis such as the Legendre Basis is necessary where modes of the basis are filtered and then transformed back. Applying this filter to the solution coefficients at each stage of RK4 removes high order content from the solution coefficients at each time step and it was demonstrated that this filter indeed provides a remedy of the aliasing instability. It was further found that only filtering at the end of the

RK4 integration provides very similar results and is computationally a much cheaper approach. Regarding the use of SGS models it can be concluded that the dynamic Smagorinsky and dynamic Heinz models do perform better than the constant coefficient Smagorinsky model for high polynomial order simulations. Higher polynomial orders are needed because the sharp modal cut-off test filter used in the dynamic models should be based on a cut-off order P_{test} that is smaller than the polynomial order of the DG method but still high enough to capture the inertial range dynamics. It was shown that for the simple Taylor-Green vortex case at $Re = 1600$ the best results have been obtained for the dynamic models with a test filter based on $P_{test} \approx (P_{grid} + 1)/2 - 1$. These dynamic model results have been obtained by applying an element based volume average to the numerator and denominator of the expression for the dynamic constant. The element based average is a general approach since the $(C_s\overline{\Delta})^2$ values still vary from element to element without assuming any statistical homogeneity of the flow. Although the dynamic models show significant improvements over the constant Smagorinsky model results, the performance gain compared to simulations without an SGS model are quite small. We believe that to test the SGS models more rigorously will require simulations at higher Reynolds numbers on comparable grids. This would increase the SGS contributions and hence the positive effect of the SGS model should become more visible. Moreover, more complex flows such as the channel flow will be considered in future studies.

References

[1]Kirby Robert M., K. G. E., "De-aliasing on non-uniform grids: algorithms and applications," 2003.

[2]Gassner Gregor J., B. A. D., "On the accuracy of high-order discretizations for underresolved turbulence simulations," 2013.

[3]Diosady Laslo T., M. S. M., "Design of a Variational Multiscale Method for Turbulent Compressible Flows," Aiaa cfd conference, NASA Ames Research Center, San Diego, CA, United states, June 2013.

[4]Garnier, E., Adams, N., and Sagaut, P., *Scientific Computation: Large Eddy Simulation for Compressible Flows*, Springer, 2009.

[5]Heinz, S. and Gopalan, H., "Realizable versus non-realizable dynamic subgrid-scale stress models," *Physics of Fluids*, Vol. 24, 2012.

[6]Wang, D. Z., "1st International Workshop on High-Order CFD Methods," .

[7]Brazell, M. J. and Mavriplis, D. J., "3D mixed element discontinuous Galerkin with shock capturing," San Diego, CA, United states, 2013, p. American Institute of Aeronautics and Astronautics (AIAA).

[8]Lax, P. D., "Weak solutions of nonlinear hyperbolic equations and their numerical computation," *Communications on Pure and Applied Mathematics*, Vol. 7, No. 1, 1954, pp. 159–193.

[9]Shahbazi, K., Mavriplis, D., and Burgess, N., "Multigrid algorithms for high-order discontinuous Galerkin discretizations of the compressible Navier-Stokes equations," *J. Comput. Phys. (USA)*, Vol. 228, No. 21, 2009/11/20, pp. 7917 – 40.

[10]Hartmann, R. and Houston, P., "An optimal order interior penalty discontinuous Galerkin discretization of the compressible Navier-Stokes equations," *J. Comput. Phys. (USA)*, Vol. 227, No. 22, 2008/11/20, pp. 9670 – 85.

[11]Jameson, A., Schmidt, W., and Turkel, E., "Numerical solutions of the Euler equations by finite volume methods using Runge-Kutta time-stepping schemes," 1981.

[12]Kirby, A. C. and Mavriplis, D. J., "An Adaptive Explicit 3D Discontinuous Galerkin Solver for Unsteady Problems," .

[13]Blackburn, H. M. and Schmidt, S., "Spectral element filtering techniques for large-eddy simulation with dynamic estimation," *J. Comput. Phys.*, Vol. 186, 2003, pp. 610–629.

[14]Pope, S. B., *Turbulent Flows*, Press Syndicate of the University of Cambridge, 2000.